Micellar Structures of Block-Copolymers with Ordered Cores in Dilute Solution as Studied by Polarized and Depolarized Light Scattering

SHAOLIANG LIN,[1,2] JIAPING LIN,[2] TAKUHEI NOSE,[1] TOMOKAZU IYODA[3]

[1]Department of Nanochemistry, Tokyo Polytechnic University, Atsugi-shi, Kanagawa 243-0297, Japan

[2]Key Laboratory for Ultrafine Materials of Ministry of Education, School of Materials Science and Engineering, East China University of Science and Technology, Shanghai 200237, China

[3]Chemical Resources Laboratory, Tokyo Institute of Technology, CREST(JST), Nagatsuta, Yokohama, Japan

Received 31 October 2006; accepted 18 January 2007
DOI: 10.1002/polb.21135
Published online in Wiley InterScience (www.interscience.wiley.com).

ABSTRACT: The hierarchical self-assembly behaviors of a series of amphiphilic liquid crystalline block copolymers (pEG_mAz_n), consisting of poly(ethylene glycol) (*pEG*) block and liquid crystalline polymer block (*pAz*) of poly{*11*-[*4*-(*4*-butylphenylazo) phenoxy]-undecyl methacrylate} containing an azobenzenzene mesogen, in the selective solvent diethyleneglycol, which is good for *pEG* block, were studied by polarized and depolarized light scattering. It was found that these copolymers can form micellar particles with internal ordered structures of optical anisotropy. Depending on the relative lengths of the blocks, the obtained micellar structures show optical anisotropies with different geometrical anisotropies. The higher composition of *pAz*-core blocks leads to the larger aggregate. The lower-molecular-weight copolymers tend to form the long and thin strings, which show rather the larger size with larger aggregation number. Even at the similar composition of *pAz*-core block, copolymers with different chain lengths can form the core of the different aggregating structures with the different molecular orientations. It was also found that the addition of a small amount of the surfactant, $C_{12}E_{25}$, makes the string-like aggregate shorter. © 2007 Wiley Periodicals, Inc. J Polym Sci Part B: Polym Phys 45: 1333–1343, 2007
Keywords: light scattering; micelles; self-assembly; ordered structure

INTRODUCTION

Recently, hierarchical self-assembly of amphiphiles, polymer, copolymer, and their complexes has received much attention, and is a powerful tool for producing functional materials, such as smart membranes, tunable nanoporous materials, and optoelectronic devices.[1–5] Among these, because of mesogenic property, liquid crystalline (LC) polymer and its copolymers containing rod-like or disc-like mesogen play an important role to give fine order structures to construct more functional supramolecular particles and higher-order hierarchical assemblies at different length scales and anisotropic properties, which can be found in the several reviews.[2,3,6,7] For instance, Lee et al. have reported that rod-coil diblock molecules based on an elongated rod can hierarchically assemble into 3D honeycomb-like supromolecular structure and coil-rod-coil triblock molecules self-assemble into discrete cylinders that organize into a 3D tetragonal superlattice.[8–10] Li et al. have studied the hierarchical assembly of a series of rod-coil diblock copolymers, poly(styrene-block-(2,5-bis-[4-methoxyphenyl]

Correspondence to: S. Lin (E-mail: linshaoliang@hotmail.com)

Journal of Polymer Science: Part B: Polymer Physics, Vol. 45, 1333–1343 (2007)

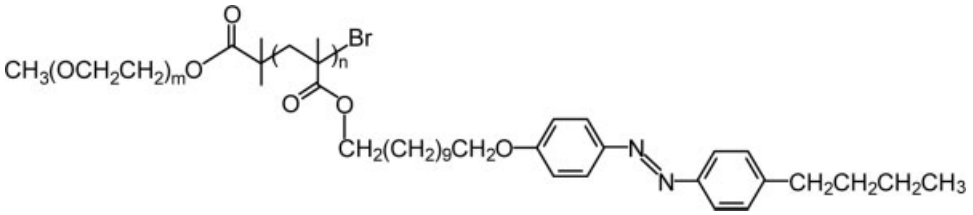

Figure 1. Chemical structure of the block copolymer, pEG_mAz_n.

oxycarbonyl) styrene). It was found that block copolymers microphase separate into ordered structures and PMPCS blocks form supramolecular columnar nematic phase within the microphase-separated block copolymers.[11]

The hierarchical self-assembly of amphiphilic copolymers in solution has also been reported.[12–16] It was shown by Nolte et al. that amphiphilic diblock copolymer constructed from a hydrophilic block of isocyanopeptides and a hydrophobic block of polystyrene can self-assemble in a hierarchical fashion to form rod-like micelles, vesicles, and even helical and double helical aggregates in water.[12] Lodge et al. have reported the formation of multicompartment micelles formed by ABC triblock terpolymers in aqueous media.[15,17,18] They observed disk-like fluorocarbon (A) domains sandwiched by two layers of hydrocarbon (B), while the hydrophilic blocks (C) emanate from the disk/disk interfaces. Such a fine internal structure in micelle was also found by the ABC triblock complex with diblock copolymer in water.[16] However, the hierarchical self-assembly of amphiphilic LC copolymers with ordered architecture has not been extensively investigated in dilute solution.

On the other hand, light scattering has been extensively applied to dynamics studies of particles in solution.[19–26] Especially *depolarized* light scattering can access information about not only size but also shape of micelle.[24–26] It has not become a very common technique to investigate micelle shape because of the weakness of the depolarized signal compared with the polarized signal.

In this work, the hierarchical self-assembly behaviors of a series of amphiphilic LC block copolymers in dilute solution are studied by using polarized and depolarized light scattering. Because of molecular orientation of LC blocks in the core, the high depolarized intensity of micelles can be obtained, which is suitable to study the micelle size and structure by this approach. Block-length dependencies of particle shape and optical anisotropy are investigated. The influence of introduction of a small amount of surfactant on the micelle size and shape is also studied.

EXPERIMENTAL

Materials

A series of amphiphilic LC block copolymers (pEG_mAz_n), consisting of poly(ethylene glycol) (*pEG*) block and LC polymer block of poly{*11*-[*4*-(*4*-butylphenylazo) phenoxy]-undecyl methacrylate} containing an azobenzene (*Az*) mesogen, with various degrees of polymerization (m, n), were synthesized by using the atom transfer radical polymerization method. The pEG_mAz_n exhibit microphase-separated structures with the *Az* blocks forming LC matrices. The synthesis and some basic properties in bulk for the sample materials have been described in detail elsewhere.[27] The chemical structure of the block copolymer, pEG_mAz_n, is shown in Figure 1, and the characteristics of the materials used here are listed in Table 1.

The selective solvent, diethyleneglycol (DEG), was purchased from Sigma and used without further purification. To control a micelle size, we added a small amount of the nonionic surfactant, poly(etylene glycol) monododecyl ether ($C_{12}E_{25}$) with 25 ethylene glycol units, which was purchased from Nikko Chemicals and used as received.

Preparation of Micelle Solutions and Thermal Treatments

The copolymer was first dissolved in tetrahydrofuran (THF), a common solvent for both *pEG* and *pAz* blocks, and optically purified by Millipore filters of nominal pore size of 0.2 μm, to give a stock solution. A desired amount stock solution was added dropwise to the selective solvent, DEG, with stirring at 40 °C. The solution was stirred for 8 h to make sure that it is homogeneous, and then evaporated under mild vacuum at 50 °C for 3 h to remove

Table 1. Code Names and Characteristics of Block Copolymers and Their Solutions

Code Name	Composition (m:n)	M_w (NMR) ($\times 10^4$)	Az (wt %)	Concentration (wt %) ($\times 10^{-3}$)
$pEG_{454}Az_{135}$	454:135	8.64	72	3.96
$pEG_{454}Az_{82}$	454:82	6.03	67	3.94
$pEG_{454}Az_{34}$	454:34	3.67	46	10.8
$pEG_{114}Az_{18}$	114:18	1.39	64	3.96
$pEG_{40}Az_{10}$	40:10	0.69	71	2.12
$pEG_{40}Az_{10}$/S	$C_{12}E_{25}$-6.5 wt %[a]	–	–	2.43

[a] The mixture with $C_{12}E_{25}$ of 6.5 wt % (mixed composition) as surfactant.

THF. Subsequently, such a micelle solution was stirred for 4 h, partially transferred into an optical light scattering cell, and sealed.

For preparation of surfactant-mixed solution, we added a desired small amount of $C_{12}E_{25}$ to make the THF solution of a mixture of $pEG_{40}Az_{10}$ and $C_{12}E_{25}$ in the first step mentioned above. The composition of $C_{12}E_{25}$ in the total solute, $pEG_{40}Az_{10}$ and $C_{12}E_{25}$, was 6.5 wt %.

The concentrations of prepared solution used for the light scattering measurements are also listed in Table 1. The sealed cell containing micelle solution is annealed at 130 °C for 2 h and cooled down to a setting temperature. The stability of micelle size for $pEG_{454}Az_{34}$ at different setting temperature is shown in Figure 2. As it can be seen, at 30 °C the hydrodynamic radius R_h (measured at the scattering angle 45°) is increased dramatically after 3 days. On the other hand, R_h at 50 °C is still stable even after 10 days. Hereafter, after annealing at 130 °C for 2 h, the cell containing micelle solution for all pEG_mAz_n samples is cooled down to 50 °C and kept for light scattering measurement.

Light Scattering Measurements

Light scattering was measured by a laboratory-made apparatus equipped with an ALV-High QE APD detector and an ALV-5000 digital correlator using a He-Ne laser (the wavelength λ of 633 nm) as a light source.

Polarizer and analyzers used were conventional ones, and the optical leak of polarizers were examined by using polystyrene latex solution to be less than 0.05% of scattered light under the crossed position of polarizers. Depolarized intensity observed here was about 10% and much higher than the leak.

In dynamic light scattering, the correlation function, $G_1(t)$, of electric field was calculated from the autocorrelation function, $G_2(t)$, of scattered light intensity by the equation for homodyne

$$G_2(t) = A(1 + B|G_1(t)|^2) \quad (1)$$

where A and B are constants. $G_1(t)$ reasonably allowed us to obtain the decay rate, Γ, by the second-order cumulant method, where the correlation function is expressed as

$$\ln(G_1(t)) = -\overline{\Gamma}t + \frac{\mu_2}{2}t^2 + \cdots \quad (2)$$

where $\overline{\Gamma}$ and μ_2 are the average decay rate and the variance of the distribution of decay rates, respectively. The polydispersity index P is defined as the ratio of the variance μ_2, to the square of $\overline{\Gamma}$:

$$P = \frac{\mu_2}{\overline{\Gamma}^2} \quad (3)$$

The polydispersity indices P obtained in the present study are relatively small, for typical examples, the values P for $pEG_{114}Az_{18}$ (at a scattering angle of 40°) are 0.12 and 0.09, for VV- and

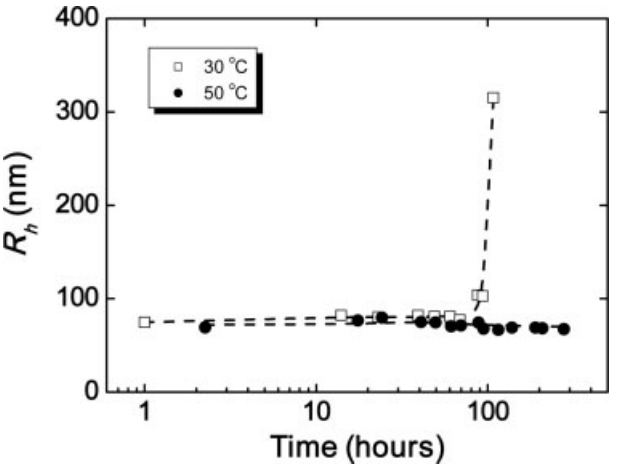

Figure 2. Time-evolution of hydrodynamic radius R_h for $pEG_{454}Az_{34}$ in DEG at 30 °C (□) and 50 °C (●).

VH-component, respectively. Therefore, we may say that the micelle-size distribution may give no serious effects on data analyses, although the P dose not always reflect the size distribution only.

The viscosity, η (cp), of the solvent, DEG, necessary for calculating the hydrodynamic radius was measured with a capillary-type viscometer to be described by $\eta = 5.91 \times 10^{-5} \exp(3.90 \times 10^3/T)$ (T: absolute temperature), and the refractive index, n, of DEG was 1.45.

BACKGROUNDS FOR DEPOLARIZED LIGHT SCATTERING AND TRANSLATIONAL AND ROTATIONAL DIFFUSION OF AXIALLY SYMMETRIC PARTICLES

The decay rates, Γ_{VV} and Γ_{VH}, for scattered light of VV- and VH-components are, respectively, written as follows:

$$\Gamma_{VH} = 6\Theta + Dq^2 \tag{4}$$

and

$$\Gamma_{VV} = D(q^2 + 6\Theta k) \tag{5}$$

where the VV- and VH-component, respectively, denote the vertically and horizontally polarized scattered light for the vertically polarized incident light beam; the wave number, q, is defined $q = (4\ \pi n/\lambda)\sin(\theta/2)$, with scattering angle θ; D is the translational diffusion coefficient, Θ is the rotational diffusion coefficient of the particles, and k is a constant depending on the character of optical anisotropy of the particles, which should be zero when the particle has no anisotropy.

One can see from eq 4 that the slope and intercept (at $q^2 = 0$) of plots of Γ_{VH} against q^2 give translational and rotational diffusion coefficients, respectively. It should be noted that the rotational diffusion coefficient by depolarized light scattering depends on the anisotropic polarizability (tensor) in the molecular coordinates of nonspherical particles, in general.

Suppose prolate or oblate particles with the long and short semiaxis lengths being a and b. Then, translational diffusion coefficient, D, and rotational diffusion coefficient, Θ, are respectively, written in the forms of

$$D = \frac{k_B T}{6\pi\eta a} f_t(b/a) \tag{6}$$

and

$$\Theta = \frac{k_B T}{8\pi\eta a^3} f_r(b/a) \tag{7}$$

The functions $f(a/b)$ of the axial ratio a/b are to be unity at $a/b = 1$, that is when the particle is spherical. The hydrodynamic radii, R_t and R_r, of translational diffusion and rotational diffusion are, respectively, defined as

$$R_t = \frac{k_B T}{6\pi\eta D} \tag{8}$$

and

$$R_r^3 = \frac{k_B T}{12\pi\eta\Theta} \tag{9}$$

such that both of the hydrodynamic radii defined here should be equal to the geometrical radius, respectively, at $a = b$, that is in the case of sphere. Here, k_B is the Boltzmann constant, and η is the solvent viscosity. The following equations are obtained from the eqs 6–9 of definitions, which give alternative relations among these quantities defined.

$$\frac{a}{R_t} = f_t(b/a) \tag{10}$$

$$\frac{a^3}{R_r^3} = \frac{3}{2} f_r(b/a) \tag{11}$$

We also have the following relation.

$$\frac{R_r}{R_t} = f_t(b/a)\left[\frac{3}{2} f_r(b/a)\right]^{-1/3} \tag{12}$$

Rotational diffusion has two elements: those of rotations around the axis of parallel or perpendicular to the symmetrical axis, referring to as $\Theta_\perp$ and $\Theta_{/\!/}$. Even if the geometrical shape is the same, rotational decay rate measured by depolarized light scattering depends on the direction of optical anisotropy relative to the geometrical anisotropy. When the optical and geometrical normal axes are common, we have two cases that the major polarizability axis is parallel or perpendicular to the geometrical major axis of length a. For these two cases, we have the expressions for relations between observed rotational diffusion coefficient.

$$\Theta = \frac{2}{3}\Theta_\perp \quad \text{(parallel)} \tag{13}$$

$$\Theta = \frac{1}{3}(\Theta_\perp + \Theta_\parallel) \quad \text{(perpendicular)} \tag{14}$$

The ratio of R_r to R_t, R_r/R_t, depends on the shape of particles as well as the direction of optical anisotropy relative to the geometrical major axis. Therefore, we have useful information about particle

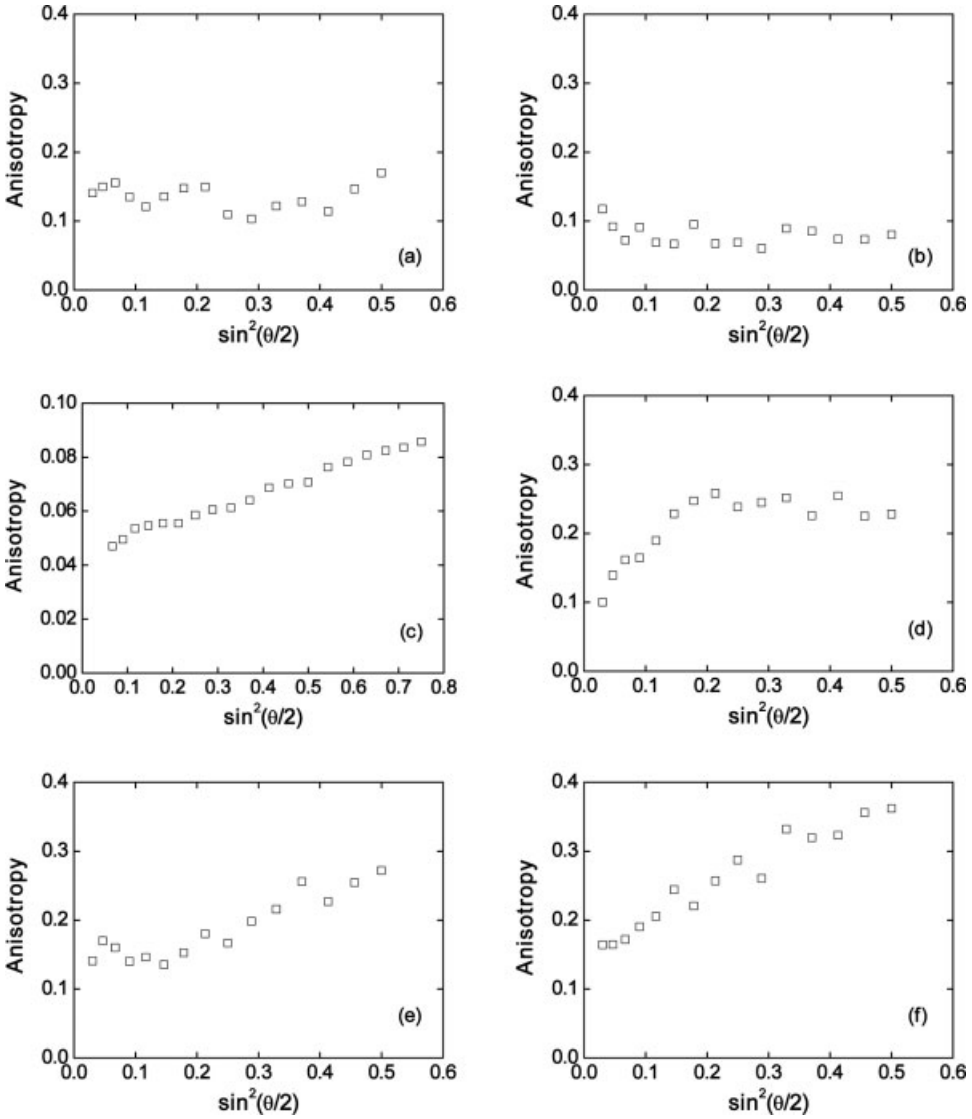

Figure 3. Optical anisotropy expressed by the ratio, I_{VH}/I_{VV}, of depolarized to polarized scattered intensities for various micelles as a function of $\sin^2(\theta/2)$. (a) $pEG_{454}Az_{135}$; (b) $pEG_{454}Az_{82}$; (c) $pEG_{454}Az_{34}$; (d) $pEG_{114}Az_{18}$; (e) $pEG_{40}Az_{10}$; (f) $pEG_{40}Az_{10} + C_{12}E_{25}$ (6.5 wt %).

structures from the ratio experimentally observed. Since the functions f_t and f_r are given for prolate and oblate ellipsoids, we can calculate the ratio of R_r/R_t as a function of a/b for the four cases, prolate and oblate shapes combined with parallel and perpendicular optical axes. The ratio of a/R_t is given as a function of a/b as well. They are shown in Figures A2 and A3 in Appendix, respectively.

RESULTS AND DISCUSSION

Depolarized and Polarized Light Scattering Analyses

Because of amphiphilic characteristics, pEG_mAz_n copolymer in the selective solvent, DEG, can self-assemble to form micelles. On the other hand, according to the ref. 27, the homopolymer *pAz* can exhibit LC property in the bulk state even the temperature is larger than 50 °C. The formation of LC phase for the pEG_mAz_n copolymer can also be found in the bulk state. Such a natural mesogenic property may induce *pAz* blocks to form LC phase within the micelle, which may give optical anisotropy to the particles. Such an optical anisotropy can be expressed by the ratio, I_{VH}/I_{VV}, of depolarized to polarized scattered intensities in the static light scattering. Optical anisotropies for various micelles as a function of $\sin^2(\theta/2)$ are shown in Figure 3. The compositions for micelles are presented

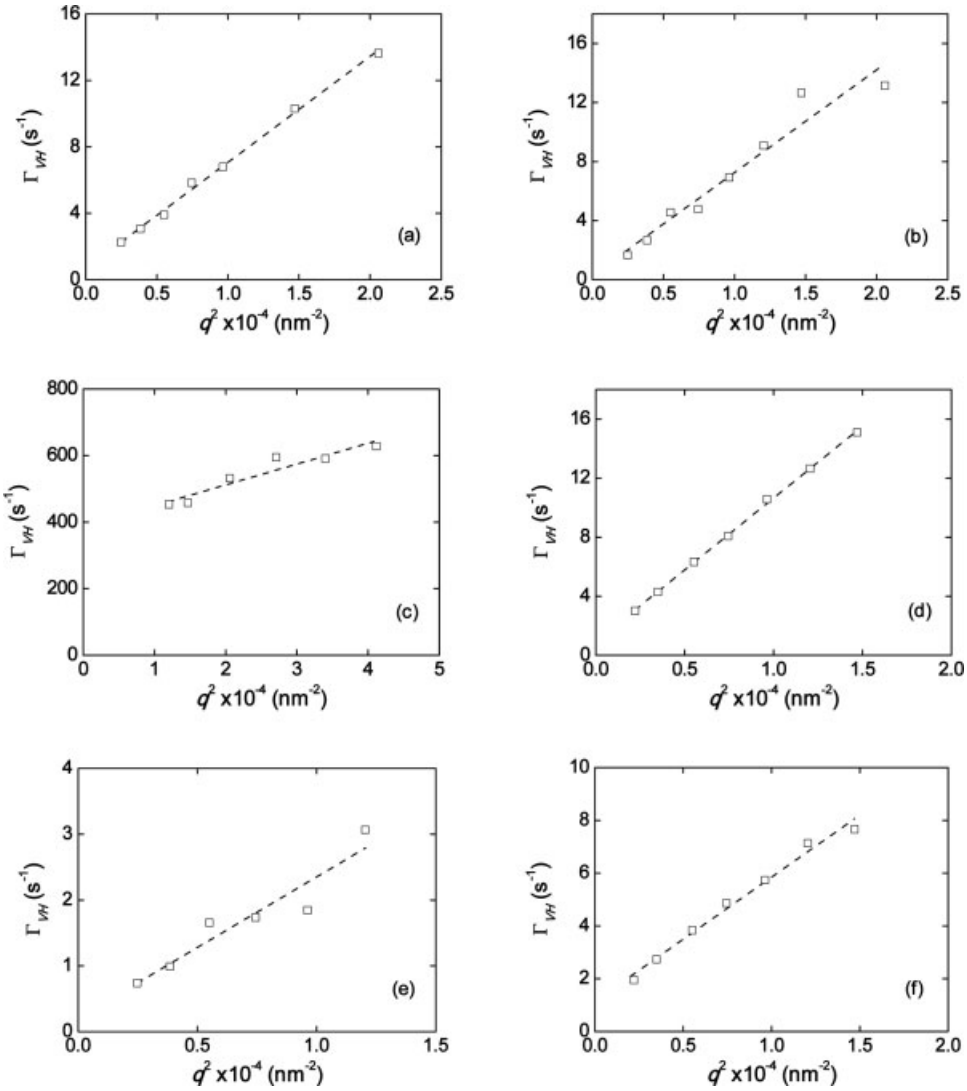

Figure 4. Plots of VH-decay rate, Γ_{VH}, against q^2 for various micelles. (a) $pEG_{454}Az_{135}$; (b) $pEG_{454}Az_{82}$; (c) $pEG_{454}Az_{34}$; (d) $pEG_{114}Az_{18}$; (e) $pEG_{40}Az_{10}$; (f) $pEG_{40}Az_{10} + C_{12}E_{25}$ (6.5 wt %).

in the caption. One can see in Figure 3 the most anisotropies of various micelles are larger than 10%. The appreciable VH-intensities observed are strong enough to measure the dynamic light scattering. Meanwhile, such higher anisotropy suggests that ordered structure is formed within

Table 2. Results of Depolarized (VH) Light Scattering

Code Name	Anisotropy at $\theta = 30^\circ$	R_t (μm)	R_r (μm)	R_r/R_t	Length $2a$ (μm)	Thickness $2b$ (μm)
$pEG_{454}Az_{135}$	0.15	0.36	0.47	1.3_0	1.6	0.36
$pEG_{454}Az_{82}$	0.072	0.33	0.61	1.8_5	2.7	0.090
$pEG_{454}Az_{34}$	0.055	0.036	0.056	1.5_6	0.22	0.020
$pEG_{114}Az_{18}$	0.12	0.23	0.42	1.8_3	1.8	0.080
$pEG_{40}Az_{10}$	0.16	1.06	0.69	0.63	6.9	0.54
$pEG_{40}Az_{10}$/S	0.17	0.48	0.39	0.81	2.6	0.72

micelles because of the alignment of azobenzene moieties. As observed in Figure 3, the dependence of strength of anisotropy on scattering angle can be found in some cases, such as micelles formed by $pEG_{454}Az_{34}$ and $pEG_{40}Az_{10} + C_{12}E_{25}$ (6.5 wt %), shown in Figure 3(c,f), respectively. The anisotropy, I_{VH}/I_{VV}, increases with increasing the scattering angle, which may suggest that the micelle with internal ordered structure shows some flexibility.

Figure 4 shows the plots of VH-decay rate, Γ_{VH}, against q^2 for various micelles. The plots are approximately linear to evaluate the intercept (6Θ) and slope (D), giving translational and rotational diffusion coefficients according to eq 4. However, the accuracy of rotational diffusion for some micelle solutions is not so good because of small values of intercept. Reliability of analysis is still open, because the measurements are in the range of $qR > 1$. The characteristics for various micelles evaluated from D and Θ by eqs 8 and 9 are listed in Table 2, where the calculated values of hydrodynamic radii, R_t and R_r, of translational diffusion and rotational diffusion, respectively, and the ratio of R_r to R_t, are presented.

We make analyses for VV-components of static and dynamic light scattering to see reliability of the above results by checking their consistencies. By the Guinier plots (log I vs. q^2) for angular dependence of VV-scattered light intensity, we obtained the intensity at the zero angle, I(0), and the initial slope of the plot. The intensity I(0) was divided by the concentration C and the square of the weight fraction (W) of pAz block in pEG_mAz_n to be the reduced intensity, $I(0)/(CW^2)$, which may be a measure of the molecular weight of the micelle, under the approximation of optically invisible pEG-block in DEG (Note: In this approximation, the refractive index increment is proportional to W). The initial slope may be put approximately to be $R_g^2/3$, with R_g being the radius of gyration of the core of Az block. The results of reduced intensity, $I(0)/(CW^2)$, and apparent R_g for various micelles are list in Table 3. The hydrodynamic radii, R_h(VV), calculated from the polarized (VV) light scattering, for various micelles are also presented in Table 3. Comparing R_h(VV) with R_t, one can see that the values of R_h(VV) are close to R_t obtained by the VH analysis. The reduced intensity, $I(0)/(CW^2)$, is consistent with the particle size. Meanwhile, we can observe that R_g for various micelles show the same order of the size evaluated by dynamic light scattering. So the VV-scattering data shown in Table 3 support the above analyses of VH-scattering.

Table 3. Results of Polarized (VV) Light Scattering

Code Name	R_g (μm)	$I(0)/CW^2$ (a.u.)	R_h(VV) (μm)	R_t (μm)
$pEG_{454}Az_{135}$	0.23	0.58	0.32	0.36
$pEG_{454}Az_{82}$	0.20	1.20	0.37	0.33
$pEG_{454}Az_{34}$	0.078	0.011	0.032	0.036
$pEG_{114}Az_{18}$	0.27	0.89	0.24	0.23
$pEG_{40}Az_{10}$	0.32	1.63	1.08	1.06
$pEG_{40}Az_{10}$/S	0.28	2.84	0.44	0.48

Estimation of Particle Shapes from Radii of Translational and Rotational Diffusion Coefficients

As we mentioned earlier, depolarized light scattering provides the rotational and the translational diffusion coefficient. Furthermore, these parameters can be used together with hydrodynamic theories to access information about not only the size but also the shape of the micelles in solution. As seen from Figure A2, the R_r/R_t value of larger than about 1.2 indicates the elongated micelles are prolate ellipsoids with the molecular orientation parallel to the elongation axis. The R_r/R_t value of less than unity suggests the elongated micelles are prolate ellipsoids with the molecular orientation perpendicular to the elongation axis. Furthermore, the ratio deviates from unity more, the ellipsoid is a more elongated. As listed in Table 2, The R_r/R_t values of the various micelles formed by $pEG_{454}Az_{135}$, $pEG_{454}Az_{82}$, $pEG_{114}Az_{18}$, and $pEG_{454}Az_{34}$, are larger than 1.3, which suggests these micelles are prolate ellipsoids with the molecular orientation parallel to the elongation axis. In contrast, the micelle formed $pEG_{40}Az_{10}$ and the mixture micelle formed by $pEG_{40}Az_{10}$ and surfactant are prolate ellipsoids with the molecular orientation perpendicular to the elongation axis, owing to the R_r/R_t value being less than 1.0.

If we can assume these types of ellipsoids for the micelle, we can evaluate the major and minor axis lengths of the ellipsoid from the ratio of R_r/R_t and R_t. If we take the micelle formed by $pEG_{454}Az_{135}$ (Table 2), for example, the R_r/R_t value of 1.30 suggests the axis ratio, a/b, to be 4.43 from Figure A2, and then Figure A3 gives $a/R_t = 2.23$ for $a/b = 4.43$, and from $R_t = 0.36$ μm, we have the estimated length, $2a$, and thickness, $2b$, to be 1.6 μm and 0.36 μm, respectively. The estimated axis lengths thus obtained are listed in Table 2. Reminded the experimental accuracy of obtaining R_r and R_t, we cannot take the estimated lengths so serious but only the order of length.

On the other hand, the stretched main chain length of pEG_mAz_n is roughly estimated from the chemical structure as follows. The lengths of *pEG*-moieties of 114 and 454 units are about 41 and 163 nm, respectively, if we approximate the PEO-unit length to be 0.36 nm. While the *Az* units from 34 to 135 correspond to the length of 9–34 nm, with the unit length of *Az*-containing block being approximated 0.25 nm. The thicknesses, 2b, estimated from experiments for these micelles ($m = 114$ and 454) (Table 2) are in the range of value expected from molecular structure. So, these micelles may be elongated rod-like particle.

The micelles of $pEG_{40}Az_{10}$ (the smallest unimer) with and without surfactant exhibit quite different behavior, forming very large micelle having the R_r/R_t value less than unity (Table 2). Considering that the stretched lengths of the unimer is around 16 nm, which is much thinner than the estimated thickness of *b* expected based on the elongated ellipsoid, these two micelles are not a solid elongated ellipsoid. The small unimers may be associated progressively and linearly forming the core by *Az*-blocks, so that more likely structure is not a large rigid rod, but is rather a long string-like micelle, which is somehow coiled to form an ellipsoidal nonsolid particle as a whole. Otherwise, it might be a multilaminated solid particle. However, the string-like structure may be more likely, because PEO-block has enough solubility for the solvent DEG.

Block-Length Dependence of Micellar Structures

pEG_mAz_n copolymers in DEG can form micellar structures with different molecular orientations. The various components of *pEG* and *Az* moieties play a dominant role on the micellar structures and particle size. As seen in Table 2, the higher composition of core blocks [*Az* (wt %) shown in Table 1] leads to the larger aggregate (larger R_t) as usually expected. Meanwhile, typical results of anisotropy of various micelles measured at 30° are also shown in Table 2, as observed that the larger anisotropy can be obtained for higher composition of core blocks. On the other hand, the micelles formed by the lower-molecular-weight copolymers show rather the larger size with larger aggregation number, for example, $pEG_{40}Az_{10}$.

For the similar composition of *Az*-core block, such as $pEG_{454}Az_{135}$ and $pEG_{40}Az_{10}$, the former one forms the rod micelle with the molecular orientation parallel to the elongation axis, while the later one forms a more flexible string with the molecular orientation perpendicular to the elongation axis. It suggests that even at the similar composition of *Az*-core block, the different chain lengths can form the core of the different aggregating structures with the different molecular orientations.

Comparison with micelles formed by $pEG_{40}Az_{10}$ and mixture of $pEG_{40}Az_{10}$ and $C_{12}E_{25}$, one can see in Table 2 that the addition of a small amount of the surfactant makes the string-like aggregate shorter. Meanwhile, the micelle anisotropy increases. The anisotropy of micelle formed by $pEG_{40}Az_{10}$ without surfactant exhibited as a whole shows a smaller value, because this longer string becomes more coiled due to the flexibility. The effect on the micelle structure change is similar to that observed in mixtures of C_nE_m, where, for example, the string-like micelle formed by $C_{12}E_8$ becomes shorter with adding $C_{12}E_{25}$, which forms spherical micelles in its pure aqueous solution.[28]

Additionally, azobenzene chromophore is one of the typical functional units can be applied in the fields of information storage, waveguide switching, optical memories, and so forth. Some studies on the nanostructures formed by azobenzene block copolymers have been reported.[27,29–32] They reveal that the different photophysical and photochemical behaviors are caused by the formation of nanostructures of the copolymers. In this work, the various micelles with different optical and geometrical anisotropies can be formed by the amphiphilic azobenzene block copolymers. The results can be used to produce anisotropic objects. On the other hand, the size and shape of the objects are tunable by varying the copolymer architecture, which may extend the application of azobenzene mesogens.

CONCLUSIONS

The micellization behavior of a series of amphiphilic LC block copolymers (pEG_mAz_n) in the selective solvent DEG is studied by polarized and depolarized light scattering. The block-length dependencies of micellar structures and size are carried out. Main conclusions are as follows:

1. The micellar particles with internal ordered structures of high optical anisotropy can be made of pEG_mAz_n in selective solvent. Depolarized dynamic light scattering is successfully applied, showing a high potential to investigate the particles with fine ordered structure.
2. Micellar structures formed by pEG_mAz_n highly depend on the copolymer block compositions, which can give micelles optical anisotropies with different geometrical anisotropies.

3. The higher composition of core blocks leads the larger aggregate. The micelles formed by the lower-molecular-weight copolymers show rather the larger size with larger aggregation number. Even at the similar composition of *pAz*-core block, the different chain lengths form the core of the different aggregating structures with the molecular orientations.
4. The addition of a small amount of the surfactant, $C_{12}E_{25}$, makes the string-like aggregate shorter. It reveals a potential application to control the particle size by introducing surfactant.

This work was supported by a Grant-in-Aid for "Academic Frontier" Project for Private Universities; matching fund subsidy from Ministry of Education, Culture, Sports, Science and Technology (MEXT), Japan, 2001–2005 and 2006–2008; and by National Natural Science Foundation of China (20574018, 50673026). Support from Program for New Century Excellent Talents in University in China (NCET-04-0410) is also appreciated.

APPENDIX

Translational and Rotational Diffusion of Axial-Symmetry Particles

Shown in Figure A1 are two ellipsoids constructed from an ellipse with major semiaxis a and minor semiaxis b. One, obtained by rotation about the major axis a is called a prolate ellipsoid, and the other, obtained by rotation about the minor axis b, is called oblate ellipsoid. As a/b becomes large, a prolate ellipsoid becomes a long thin rod with length $2a$ and the radius (thickness) b. While an oblate ellipsoid approaches the shape of a flat circular disk with thickness of $2b$ and radius a. According to Perrin's work,[33,34] we can obtain $f(b/a)$ for translational diffusion of such two ellipsoids.

For prolate ellipsoids,

$$f_t(b/a) = (2s)^{-1}\ln\left(\frac{1+s}{1-s}\right) \tag{A1}$$

For oblate ellipsoids,

$$f_t(b/a) = s^{-1}\tan^{-1}\left[\frac{s}{\sqrt{1-s^2}}\right] \tag{A2}$$

where the parameter s is a function of a and b, written by

$$s = \sqrt{1-b^2/a^2} \quad (\mathbf{a} \geq \mathrm{b} \text{ for any cases}) \tag{A3}$$

For rotational diffusion coefficient obtained from depolarized scattering, we need detailed diffusion behavior since the observed rotational diffusion of nonspherical particle depends on the relation between optical and geometrical anisotropies. (eqs 13 and 14).

For prolate ellipsoids, $f(b/a)$ for rotation diffusion can be written by[35]

$$f_{rX}(b/a) = \frac{3}{4s^3}\left[\frac{2s}{1-s^2} - \ln\frac{1+s}{1-s}\right] \tag{A4}$$

$$f_{rY}(b/a) = \frac{3}{4s^3}\left[-\frac{2s}{2-s^2} + \frac{1+s^2}{2-s^2}\ln\frac{1+s}{1-s}\right] \tag{A5}$$

where X and Y denote the optical and geometrical axes, respectively. As optical and giometrical axes are parallel, we can obtain

$$f_r(b/a) = \frac{2}{3}f_{rY}(b/a) = \frac{1}{2s^3(2-s^2)} \times \left[(1+s^2)\ln\frac{1+s}{1-s} - 2s\right] \tag{A6}$$

When optical and geometrical axes are perpendicular, $f_r(b/a)$ is written by

$$f_r(b/a) = \frac{1}{3}f_{rX}(b/a) + \frac{1}{3}f_{rY}(b/a) = \frac{1}{4s^3(2-s^2)} \times \left[\frac{2s}{(1-s^2)} + (2s^2-1)\ln\frac{1+s}{1-s}\right] \tag{A7}$$

For oblate ellipsoids, $f(b/a)$ for rotation diffusion can be written by[35]

$$f_{rX}(b/a) = \frac{3}{2s^3}\left[\tan^{-1}\frac{s}{\sqrt{1-s^2}} - s\sqrt{1-s^2}\right] \tag{A8}$$

$$f_{rY}(b/a) = \frac{3}{2s^3}\left[\frac{2s^2-1}{2-s^2}\tan^{-1}\frac{s}{\sqrt{1-s^2}} + \frac{s\sqrt{1-s^2}}{2-s^2}\right] \tag{A9}$$

As optical and geometrical axes are parallel, we can obtain

$$f_r(b/a) = \frac{2}{3}f_{rY}(b/a) = \frac{1}{s^3(2-s^2)} \times \left[(2s^2-1)\tan^{-1}\frac{s}{\sqrt{1-s^2}} + s\sqrt{1-s^2}\right] \tag{A10}$$

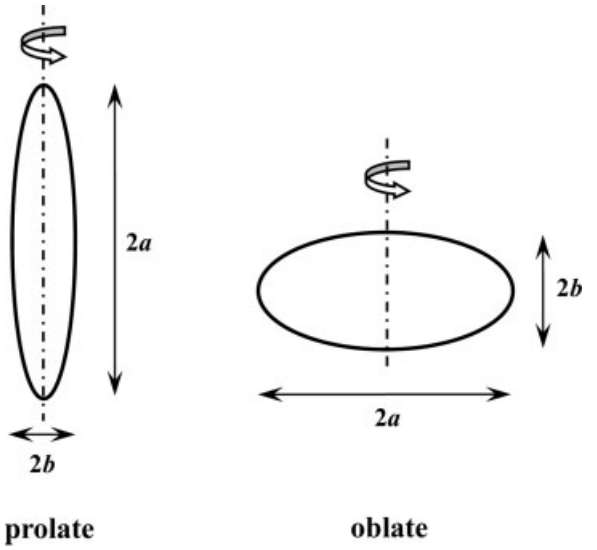

Figure A1. The layouts of prolate and oblate ellipsoids.

As optical and geometrical axes are perpendicular, we can obtain

$$f_r(b/a) = \frac{1}{3}f_{rX}(b/a) + \frac{1}{3}f_{rY}(b/a) = \frac{1}{2s^3(2-s^2)} \times \left[(1+s^2)\tan^{-1}\frac{s}{\sqrt{1-s^2}} - (1-s^2)s\sqrt{1-s^2}\right] \quad \text{(A11)}$$

The relationship between the ratio, R_r/R_t, and a/b for the four cases, prolate and oblate shapes combined with parallel and perpendicular optical axes to geometrical major axis is illustrated in Figure A2, which is drawn from eq 12 with eqs A1, A2, A6, A7, A10, and A11. While Figure A3 was drawn from eq 10 with eqs A1 and A2, which shows a/R_t of prolate and oblate ellipsoids as a function of a/b.

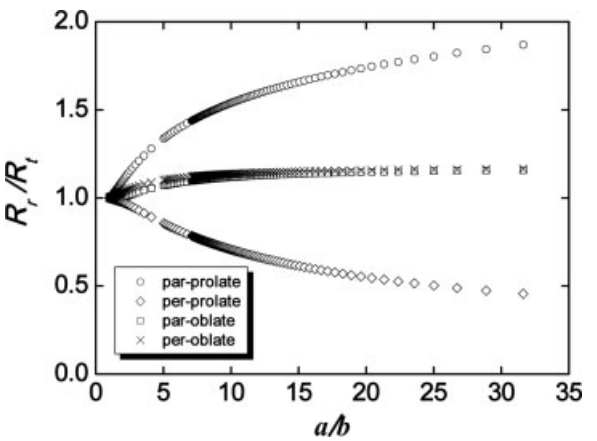

Figure A2. The plots of R_r/R_t against the axial ratio a/b for various ellipsoids: prolate ellipsoids as optical and geometrical axes are perpendicular (◇) and parallel (○); oblate ellipsoids as optical and geometrical axes are perpendicular (×) and parallel (□).

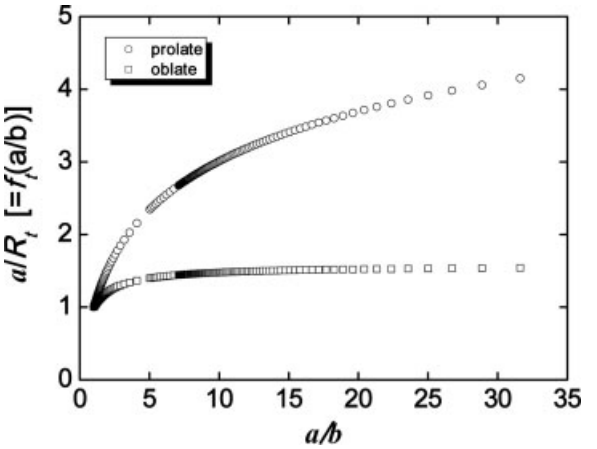

Figure A3. The plot of a/R_t ($= f(a/b)$) versus the axial ratio a/b for prolate (○) and oblate (□) ellipsoids.

Equations for rotational diffusion have been derived cylindrical rod-like molecules in approximate, analytical forms.[36–40] The results are similar to those of the present ellipsoidal bodies.

REFERENCES AND NOTES

1. Ikkala, O.; ten Brinke, G. Science 2002, 295, 2407.
2. Tschierske, C. J Mater Chem 2001, 11, 1.
3. Elemans, J. A. A. W.; Rowan, A. E.; Nolte, R. J. M. J Mater Chem 2003, 13, 2661.
4. Mezzenga, R.; Ruokolainen, J.; Fredrickson, G. H.; Kramer, E. J.; Moses, D.; Heeger, A. J.; Ikkala, O. Science 2003, 299, 1872.
5. Ikkala, O.; ten Brinke, G. Chem Commun 2004, 2131.
6. Lee, M.; Cho, B. K.; Zin, W. C. Chem Rev 2001, 101, 3859.
7. Kumar, S. Chem Soc Rev 2006, 35, 83.
8. Lee, M.; Cho, B. K.; Jang, Y. G.; Zin, W. C. J Am Chem Soc 2000, 122, 7449.
9. Cho, B. K.; Lee, M. J Am Chem Soc 2001, 123, 9677.
10. Lee, M.; Cho, B. K.; Ihn, K. J.; Lee, W. K.; Oh, N. K.; Zin, W. C. J Am Chem Soc 2001, 123, 4647.
11. Li, C. Y.; Tenneti, K. K.; Zhang, D.; Zhang, H.; Wan, X.; Chen, E.; Zhou, Q.; Carlos, A. O.; Igos, S.; Xiao, B. S. Macromolecules 2004, 37, 2845.
12. Cornelissen, J. J. L. M.; Fischer, M.; Sommerdijk, N. A. J. M.; Nolte, R. J. M. Science 1998, 280, 1427.
13. Vriezema, D. M.; Hoogboom, J.; Velonia, K.; Takazawa, K.; Christianen, P. C. M.; Maan, J. C.; Rowan, A. E.; Nolte, R. J. M. Angew Chem Int Ed 2003, 42, 772.
14. Zhang, L.; Eisenberg, A. Science 1995, 268, 727.
15. Li, Z.; Kesselman, E.; Talmon, Y.; Hillmyer, M. A.; Lodge, T. P. Science 2004, 306, 98.

16. Li, Z.; Hillmyer, M. A.; Lodge, T. P. Macromolecules 2006, 39, 765.
17. Zhou, Z.; Li, Z.; Ren, Y.; Hillmyer, M. A.; Lodge, T. P. J Am Chem Soc 2003, 125, 10182.
18. Lodge, T. P.; Hillmyer, M. A.; Zhou, Z.; Talmon, Y. Macromolecules 2004, 37, 6680.
19. Berne, B. J.; Pecora, R. Dynamic Light Scattering; Wiley: New York, 1976.
20. Chu, B. Laser Light Scattering: Basic Principles and Practice, 2nd Ed.; Academic Press: Boston, 1991.
21. Massey, J.; Power, K. N.; Manners, I.; Winnik, M. A. J Am Chem Soc 1998, 120, 9533.
22. Iyama, K.; Nose, T. Macromolecules 1998, 31, 7356.
23. Zhang, G. Z.; Wu, C. Adv Polym Sci 2006, 195, 101.
24. Schillén, K.; Brown, W.; Johnsen, R. M. Macromolecules 1994, 27, 4825.
25. Wu, J.; Pearce, E. M.; Kwei, T. K.; Lefebvre, A. A.; Balsara, N. P. Macromolecules 2002, 35, 1791.
26. Lehner, D.; Lindner, H.; Glatter, O. Langmuir 2000, 16, 1689.
27. Tian, Y.; Watanabe, K.; Kong, X.; Abe, J.; Iyoda, T. Macromolecules 2002, 35, 3739.
28. Iizuka, K.; Numasawa, N.; Hiraoka, K.; Yamazaki, R.; Nose, T. J Polym Sci Part B: Polym Phys 2005, 43, 2474.
29. Mao, G.; Wang, J.; Clingman, S. R.; Ober, C. K.; Chen, J. T.; Thomas, E. L. Macromolecules 1997, 30, 2556.
30. Schneider, A.; Zanna, J. J.; Yamada, M.; Finkelmann, H.; Thoman, R. Macromolecules 2000, 33, 649.
31. Osuji, C. O.; Chen, J. T.; Mao, G. P.; Ober, C. K.; Thomas, E. L. Polymer 2000, 41, 8897.
32. Moriya, K.; Seki, T.; Nakagawa, M.; Mao, G. P.; Ober, C. K. Macromol Rapid Commun 2000, 21, 1309.
33. Perrin, F. J Phys Radium 1934, 5, 497.
34. Perrin, F. J Phys Radium 1936, 7, 1.
35. Kim, S.; Karrila, S. J. Microhydrodynamics: Principles and Selected Applications; Butterworth-Heinemann: Boston, 1991.
36. Broerama, S. J Chem Phys 1960, 32, 1626.
37. Broerama, S. J Chem Phys 1960, 32, 1632.
38. Broerama, S. J Chem Phys 1981, 74, 6989.
39. Zero, K. M.; Pecora, R. Macromolecules 1982, 15, 87.
40. Tanford, C. Physical Chemistry of Macromolecules; Wiley: New York, 1961; p 342.